EEET ECOLOGICAL ENGINEERING & ENVIRONMENTAL TECHNOLOGY

Ecological Engineering & Environmental Technology, 25(12), 233–252
https://doi.org/10.12912/27197050/194564
ISSN 2719–7050, License CC-BY 4.0

Received: 2024.10.01
Accepted: 2024.10.20
Published: 2024.11.01

Green Chemistry Biosynthesis of Calcium Oxide Nanoparticles as Antibacterial Waste Microorganisms in Waters

Sahrul Sultan[1*], Abdul Karim[1], Nur U. Permatasari[1]

[1] Department of Chemistry, Faculty of Mathematics and Natural Sciences, Hasanuddin University, Makassar, Indonesia

* Corresponding author's e-mail: sahrul.azfara@gmail.com

ABSTRACT

Calcium oxide (CaO) nanoparticles have garnered significant interest in various environmental applications, particularly in water treatment and the control of microbial pollution. This research introduces innovative strategies for water management and waste treatment through the application of advanced technology grounded in nanoscience, utilizing local resources. The primary objective of this study is to synthesize CaO nanoparticles via a green chemistry method, employing a bioreductant derived from the Bitti (*Vitex cofassus*) plant extract. This green chemistry approach is not only environmentally benign but also effective in producing stable nanoparticles with controlled dimensions. Characterization of the nanoparticles was conducted using X-ray diffraction (XRD) and scanning electron microscopy (SEM) to ascertain their crystal structure, morphology, and particle size. The results indicated that the calcium oxide nanoparticles exhibit a face-centered cubic (FCC) crystal phase, irregular surface morphology, and a spherical shape, with an average particle size of 24.87 nm. The antibacterial efficacy of calcium oxide nanoparticles was evaluated against *Escherichia coli*, with variations in nanoparticle concentrations of 1%, 3%, and 5%, resulting in average inhibition zone diameters of 9.59 mm, 10.78 mm, and 11.78 mm, respectively. The positive control (Chloramphenicol) demonstrated an inhibition zone of 12.65 mm, while the negative control (sterile water) showed no inhibition (0 mm). Similarly, for *Staphylococcus aureus*, the inhibition zone diameters with nanoparticle concentrations of 1%, 3%, and 5% were 10.26 mm, 11.15 mm, and 14.15 mm, respectively, with the positive control exhibiting an inhibition zone of 12.82 mm and the negative control showing no inhibition (0 mm). The CaO nanoparticles demonstrated greater efficacy against *Staphylococcus aureus* compared to *Escherichia coli*, exhibiting the capability to inhibit and eliminate both bacterial strains. The application of these nanoparticles as antibacterial agents presents a promising approach to effectively mitigate microbial waste in aquatic environments, suggesting their potential use as a solution for environmentally friendly microbial waste treatment.

Keywords: green chemistry, biosynthesis, calcium oxide nanoparticles, antibacterial activity, microorganism waste, water treatment

INTRODUCTION

Water pollution resulting from the effluents of microorganisms constitutes a significant environmental challenge in numerous regions worldwide (Lv et al., 2024). The presence of pathogenic microorganisms in aquatic environments not only disrupts ecosystem balance but also poses substantial health risks to both humans and animals in proximity (Takci et al., 2024). Therefore, concerted efforts to mitigate microbial contamination in these environments are essential (Li et al., 2024), particularly through the implementation of environmentally friendly methods that are both effective and efficient (Some et al., 2021). A promising solution in this regard is the application of calcium oxide (CaO) nanoparticles, which possess strong antibacterial properties and the capacity to decompose microbial pollutants in water (Shultana and Khan, 2022).

The biosynthesis of calcium oxide nanoparticles utilizing natural materials, such as plant

extracts, represents a compelling alternative to conventional chemical methods (Khan et al., 2023). Several studies have employed plant extracts as bioreductors; for instance, Mazher et al. (2023) synthesized CaO nanoparticles using the extract of *Citrullus colocynthis*, while Mbega et al. (2023) utilized (*Tulbaghia violacea*) extract in the synthesis of CaO nanoparticles with antibacterial properties. Additionally, Sharma et al. (2023) incorporated (*Cleome viscosa*) leaf extract for the synthesis of CaO nanoparticles exhibiting antioxidant activity. The biosynthesis approach offers numerous advantages, including a simplified process, cost-effectiveness, environmental sustainability, and the elimination of hazardous chemicals (Nami et al., 2022). Extracts from Vitex cofassus have demonstrated the presence of bioactive compounds that can function as bioreactors, facilitating the formation and stabilization of nanoparticles with desirable size and morphology (Ahmad et al., 2022). The application of plant extracts as reducing agents in nanoparticle synthesis aligns with the principles of green chemistry (Mbenga et al., 2023), which advocates for minimizing negative environmental impacts (Maringgal et al., 2020).

Recent studies have demonstrated that biologically synthesized CaO nanoparticles exhibit significant antibacterial activity against a variety of pathogenic microorganisms (Sharma et al., 2023). Consequently, the biosynthesis of CaO nanoparticles utilizing Bitti leaf extract not only facilitates the production of effective antibacterial agents but also reinforces the principles of sustainability in water treatment technology (Mahmoud et al., 2023). The application of CaO nanoparticles as an antibacterial agent is anticipated to yield an effective (Bôlla de Menezes et al., 2024) and sustainable solution for the treatment of microbial waste in water, thereby enhancing water quality and mitigating the adverse effects of pollution (Raza et al., 2024).

METHODS

Biosynthesis of calcium oxide nanoparticles

Limestone containing calcium oxide is sourced from limestone mining operations in the Maros district of South Sulawesi, Indonesia (Sari et al., 2022). The limestone is thoroughly cleaned using distilled water to remove any adhering impurities. Subsequently, the limestone is pulverized using a mortar until it is reduced to a smaller particle size. The limestone samples are then subjected to sun drying until all moisture is eliminated. The dried limestone is further processed with a rock material crushing apparatus (Jaw crusher) to achieve a lime-like consistency. The resultant limestone powder is subsequently sieved through a 230 mesh sieve to obtain finer particles (Jiang et al., 2019). The collected limestone powder is then calcined at 1000°C for a duration of six hours to produce pure calcium oxide powder (Li et al., 2022).

The resulting calcium oxide powder was utilized at a concentration of 5% and combined with a 5% concentration of bitti leaf (*Vitex cofassus*) crude extract. The mixture was homogenized with 20 mL of distilled water while being heated on a magnetic stirrer hotplate at 60°C (Maringgal et al., 2020). The resultant solution was subjected to centrifugation at 3500 rpm for a duration of 2 hours. Following centrifugation, the mixture was filtered using filter paper, and the precipitate obtained was dried in an oven at 70°C for 30 minutes to produce calcium oxide nanoparticles (Sharma et al., 2023). Subsequently, the oxide nanoparticles were characterized using X-ray diffraction (XRD) and scanning electron microscopy (SEM) to analyze particle size, nanocrystal morphology, and other relevant morphological characteristics (Ahmad et al., 2022).

Isolation of gram-negative (*E. coli*) and gram-positive (*S. aureus*) bacteria

Gram-negative and Gram-positive bacterial isolates were obtained from contaminated wastewater sites surrounding the Antang landfill in Manggala Village, Makassar, Indonesia (Han et al., 2019). Wastewater samples were collected using sterilized dark-colored bottles prepared in the laboratory. Subsequent analysis of the samples was conducted in the laboratory, following the preservation of wastewater samples in sample containers maintained at temperatures below 4 °C with the use of ice water, thereby preventing alterations in the sample conditions during transit (Wichmann et al., 2021).

Identification of gram-negative bacteria

The identification of gram-negative bacteria was conducted using two types of media:

enrichment media (Nutrient Broth/NB) and growth media (Eosin Methylene Blue Agar/ EMBA) (Kim et al., 2020). Isolated wastewater samples were inoculated into nutrient broth media and incubated at 37 °C for 24 hours to facilitate the proliferation of *Escherichia coli*. Following this incubation, the proliferated bacteria were transferred to Eosin Methylene Blue Agar media utilizing a scraping technique, with subsequent incubation at 37 °C for an additional 24 hours. Bacterial colonies suspected to be *E. coli* typically exhibited a diameter of 2–3 mm, presented a black coloration at the center of the colony, and displayed a greenish metallic sheen on EMBA media. Colonies of *E. coli* were subsequently harvested from the EMBA media using an inoculating needle for further biochemical testing (Xiao et al., 2024).

Biochemical test of gram-negative bacteria

Indole production test

Colonies of *Escherichia coli* bacteria were aseptically introduced into test tubes containing tryptone broth within a laminar airflow cabinet. The test tubes were subsequently incubated at 37°C for a duration of 24 hours. Following incubation, six drops of Kovacs reagent were added to the test tube containing the *E. coli* bacterial culture. The tube was then gently agitated to ensure thorough mixing of the reagent and the culture. A positive result is indicated by the presence of a red ring at the surface of the medium, which occurs due to the production of indole from the catabolism of tryptophan by *E. coli*. Conversely, a lack of color change or the appearance of a yellow layer in the medium signifies a negative result (Raj et al., 2020).

Methy Red test

Bacterial colonies cultured on EMBA media were inoculated into a test tube containing 10 mL of Methyl Red (MR) media and incubated at 37 °C for 48 hours. Following incubation, five drops of MR indicator were added to the test tube. A positive result is indicated by the presence of a red color, whereas a negative result is indicated by the presence of a yellow color (Xiao et al., 2024).

Citrate test

Bacterial colonies derived from EMBA media were incubated in test tubes containing Koser Citrate Broth (KCB) media. The combination of colonies and media was subsequently incubated at 37 °C for a duration of 96 hours. Positive test results are indicated by turbidity in the media (Wang et al., 2024).

Identification of gram-positive bacteria

The identification of gram-positive bacteria was conducted utilizing two types of media: enrichment media (Nutrient Broth/NB) and growth media (Blood Agar Plate/BAP) (Almwafy, 2020). Wastewater samples that had been isolated were subsequently introduced into the nutrient broth media. The samples were then incubated at 37 °C for 24 hours to facilitate the enrichment of Staphylococcus aureus colonies. The resulting bacterial colonies were then transferred to BAP media for solid incubation. These bacterial colonies were inoculated on agar plates and incubated at 37 °C for 24 hours. Colonies indicative of Staphylococcus aureus were characterized by the presence of a hemolytic zone on the BAP media (Garcia et al., 2021).

Biochemical test of gram-positive bacteria

Gram stain test

A small culture of *Staphylococcus aureus* bacteria was obtained using a sterilized inoculation loop. The bacteria were subsequently spread onto a clean glass slide, followed by the addition of a small amount of sterile water. The bacterial suspension on the glass slide was then leveled and allowed to air dry. Once the bacterial smear had dried, it was fixed by passing the glass slide over a Bunsen burner several times. The bacterial smears were then treated with crystal violet dye and iodine solution, followed by washing with alcohol and counterstaining with safranin. The bacteria on the glass slide were observed under a microscope at high magnification. A positive test result was indicated by the presence of round-shaped bacterial cells (cocci) appearing in purple (Li et al., 2020).

Coagulase test

The coagulase test was conducted utilizing the slow method. A sterilized test tube was supplemented with 0.5 mL of an oxalate compound. The oxalate compound was inoculated with a small quantity of bacterial colonies using a sterilized loop. The test tube, containing the mixture of colonies and oxalate compound, was

maintained at 37 °C and evaluated at 30-minute intervals for the initial 4 hours. In the absence of clot formation, incubation was extended for an additional 24 hours. A positive result is indicated by the presence of a clot within the test tube (Chandra, 2023).

Antibacterial activity test

The antibacterial activity of CaO nanoparticles was assessed utilizing the disc paper method (Nam et al., 2022). *Escherichia coli* (a gram-negative bacteria) and *Staphylococcus aureus* (a gram-positive bacteria) were initially subcultured in nutrient agar medium and subsequently incubated at room temperature for a duration of 24 hours. The evaluation of bacterial activity was conducted through the disc diffusion method. A CaO nanoparticle solution at concentrations of 1%, 3%, and 5% was prepared by dissolving CaO nanoparticle powder in sterile distilled water and stirring the mixture with a magnetic stirrer for 15 minutes. Following this, the compacted medium was inoculated with *Escherichia coli* and *Staphylococcus aureus* on its surface. Discs with a diameter of 6 mm were saturated with the nanoparticle concentration solutions (1%, 3%, and 5%), alongside a positive control of chloramphenicol (30 µL) and a negative control of distilled water. These discs were then placed in a Petri dish containing the bacterial culture medium and incubated at room temperature for 16 to 24 hours. The zone of inhibition of bacterial growth on the medium was measured using anchors (Kumar et al., 2021).

Data analysis technique

Data management and analysis techniques were employed to ascertain the particle size, crystallinity, and crystal form of calcium oxide nanoparticles utilizing the X-ray diffraction (XRD) characterization method. The particle size determination via the XRD technique is founded on the Scherrer equation, as articulated in Equation 1 (Rabiei et al., 2020).

$$D = k\,\lambda\,\beta cos\,\theta \quad (1)$$

where: D – particle size (nm), k – crystal form factor (0.9), λ – X-ray wavelength (0.15406), β – full width at Half minimum (FWHM) value (rad), θ – diffraction angle (rad).

RESULTS AND DISCUSSION

Biosynthesis of calcium oxide nanoparticles

Limestone that remains in chunk form will be mechanically processed using a hammer to reduce it to smaller grains, thereby increasing the surface area of the sample to facilitate the subsequent smoothing process. The limestone is exposed to sunlight for drying, which helps to soften the texture of the rock prior to its conversion into powder (Li et al., 2022). The pulverization process is further advanced through the use of a rock crusher (jaw crusher), which aids in the sieving process and reduces the material size. Sieving is performed using a 230 mesh screen, with the objective of eliminating smaller particles to ensure the appropriate size of limestone powder for nanoparticle synthesis. Following this, the limestone powder undergoes calcination at 1000 °C for a duration of 4 hours, aimed at transforming calcium carbonate ($CaCO_3$) into calcium oxide (Jiang et al., 2019). The resultant calcium oxide powder is depicted in Figure 1.

Calcination at 1000 °C for six hours yields a calcium oxide powder with a purity exceeding 95%, significantly surpassing that obtained at temperatures ≤ 1000 °C (Raza et al., 2024). This enhancement in purity is attributed to the influence of elevated temperatures that exceed the decomposition point of calcium carbonate, facilitating the formation of a more refined calcium oxide product (Sd et al., 2023). Furthermore, Dewi et al. (2023) elucidate that calcination at 1000 °C accelerates the reaction rate, thereby expediting the calcination process, which in turn enhances production efficiency and reduces operational costs (Dewi et al., 2023).

The biosynthesis of calcium nanoparticles utilizing bitti leaf extract within bioreactor systems is predicated on the selection of bitti leaves, which are characterized by their high concentrations of active compounds, particularly flavonoids. Flavonoids present in bitti leaves possess the capability to reduce the oxidation state of organic compound ions, such as calcium (Ca), thereby rendering them suitable biological agents for nanoparticle synthesis (Mazher et al., 2023). The mixture was subjected to heating on a magnetic stirrer hotplate at 60 °C to activate the flavonoid secondary metabolites, facilitating the reduction of Ca^{2+} ions to form Ca nanoparticles (Maringgal et al., 2020). Nami et al. (2022) suggest that the homogenization of

calcium oxide nanoparticles with bioreductors at a specified temperature enhances the uniform dispersion of nanoparticles and promotes interaction between nanoparticles and bioreductors. An initial indication of calcium oxide nanoparticle formation in the mixture can be observed through a resultant color change. In this study, a noticeable change in color was recorded before and after centrifugation (Mbenga et al., 2023). The transition from a cloudy white to a clear white hue signifies the successful formation of calcium oxide nanoparticles. This color alteration is attributed to the aggregation (clumping) and precipitation of the solution post-centrifugation, resulting in a reduction of particle size within the mixture (Nami et al., 2022). Mazher et al. (2023) elucidate that the formation of nanoparticles from a sample is indicated by a color change occurring before and after the ingredients are combined. The observed color change signifies an increment in the number of nanoparticles produced. The outcomes of calcium oxide nanoparticle biosynthesis are illustrated in Figure 2.

In Figure 2, the observed color change represents the mechanism of reduction and oxidation reactions involving calcium ions (Ca^{2+}) and flavonoid compounds. The active compounds, specifically flavonoids, present in bitti leaf extract serve to reduce calcium ions to elemental calcium (Ca^0) (Sharma et al., 2023). Flavonoids, classified as organic compounds, function as reducing agents due to the presence of hydroxyl groups (-OH) within their phenolic structures, which facilitate electron donation (Dobrzynska et al., 2020). The reaction mechanism underlying the biosynthesis of calcium oxide nanoparticles can be observed in Figure 3.

In Figure 3, flavonoids dissolved in the reaction medium interact with calcium ions. The hydroxyl group (-OH) present in flavonoids exhibits significant reactivity in reduction-oxidation (redox) reactions (Lv et al., 2024). Flavonoids possessing antioxidant properties are capable of donating electrons from their hydroxyl groups to Ca^{2+} ions. This electron

Figure 1. Display of synthesized calcium oxide nanoparticles from limestone

Figure 2. CaO-NPs biosynthesis results (a) before centrifugation (b) after centrifugation

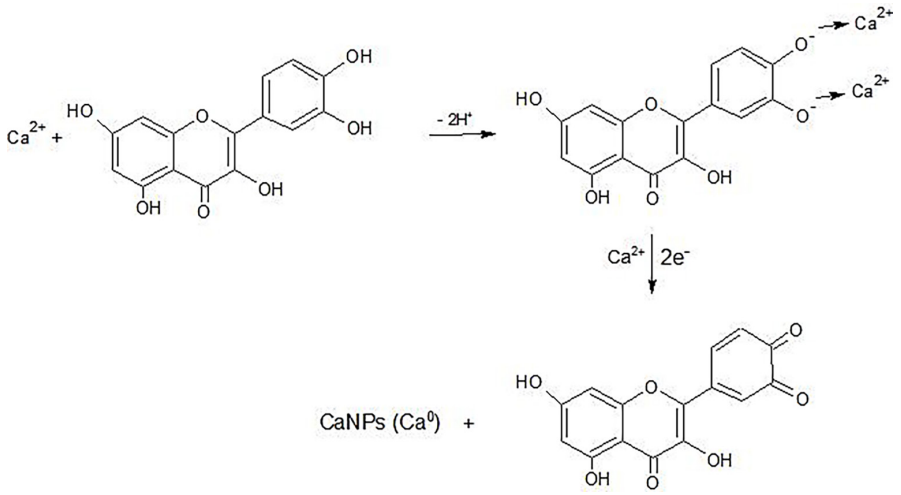

Figure 3. Biosynthesis reaction mechanism of calcium oxide nanoparticles (CaO-NPs)

transfer facilitates the conversion of the flavonoid into its oxidized form, while the Ca^{2+} ion is reduced to elemental calcium (Ca^0). Following the reduction of Ca^{2+} ions to Ca^0, these calcium atoms undergo nucleation, aggregating into small clusters (Ahmad et al., 2022). The nucleation process represents the initial stage in the formation of calcium oxide nanoparticles (CaO-NPs). Dobrzynska et al. (2020) describe that flavonoids function as stabilizing agents, preventing the further agglomeration of the already formed calcium oxide nanoparticles. The interactions that occur between flavonoids and the nanoparticle surface can inhibit excessive growth of nanoparticles, thereby maintaining the particle size at the nanoscale (Dobrzynska et al., 2020). Jadhav et al. (2022) synthesized calcium oxide nanoparticles utilizing Moringa oleifera leaf extract as an alternative biological agent for reducing calcium oxide to nanoparticles, with results indicating that Moringa oleifera leaf extract can reduce the particle size of calcium oxide to 32.08 nm, as determined by scanning electron microscopy (SEM) and X-ray diffraction (XRD) analysis. Similarly, a study conducted by Meshkatalsadat and Mehdi (2023) employed *Pistacia atlantica* leaf extract as a bioreductor for calcium oxide nanoparticles, yielding particle sizes ranging from 30 to 100 nm, as analyzed by Fourier-transform infrared spectroscopy (FTIR), SEM, and XRD techniques. Thus, calcium oxide nanoparticles can be synthesized using various plant sources, particularly those capable of reducing the oxidation state of the target ion.

Characteristics of calcium oxide nanoparticles

Characterization of CaO nanoparticles using X-ray diffraction

Characterization of calcium oxide nanoparticles was conducted utilizing X-ray diffraction (XRD) instruments to ascertain the diffraction pattern of the nanoparticles, thereby facilitating the identification of their crystal structure, phase, and particle size (Harsha Hebbar et al., 2018). According to El-Sherif et al. (2023), the analysis of nanoparticles through XRD also serves to evaluate the level of crystal clarity of the synthesized nanoparticles and to verify their purity by observing alterations in the structure of the resultant material. Diffraction patterns were acquired from sample measurements employing a Shimadzu XRD-7000 X-ray diffractometer, utilizing a Cu-Kα radiation source (λ = 1.54 Å) and a rotating angle range (2Θ) of 5–70 degrees (El-Sherif et al., 2023). The diffraction pattern of calcium oxide nanoparticles (T = 1000 °C, t = 6 hours) is illustrated in Figure 4.

The diffraction peak values (I/I0) of the intensity of the 2Θ region in Figure 4, respectively, can be seen in Table 1.

Based on Figure 4, the diffraction pattern (I/I0) of the intensity in the 2Θ region for calcium oxide nanoparticles, utilizing a wavelength of 1.540600 Å, exhibits varying peak intensities across several phases (Sari et al., 2022). The predominant diffraction peak is observed at 2Θ = 34.16°. Furthermore, additional peaks are detected at the following angles: 2Θ = 18.04°, 28.74°, 29.44°, 36.95°, 39.41°, 43.18°, 47.19°, 48.55°, 50.88°, 54.43°, 59.47°, 62.67°, and 64.39°.

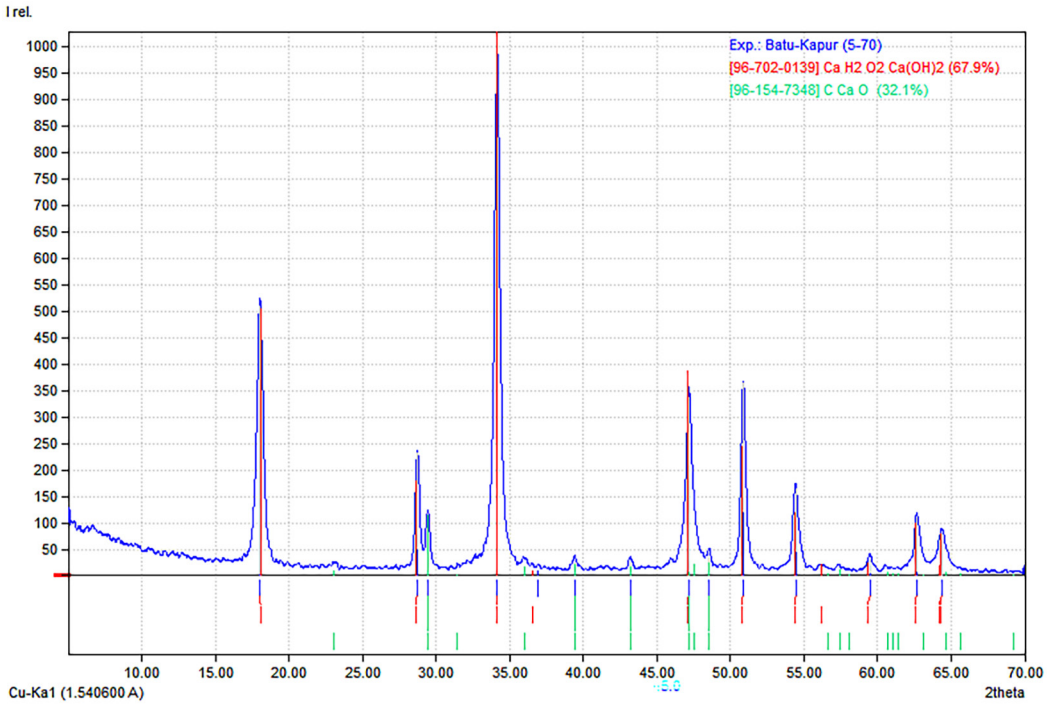

Figure 4. Diffraction pattern of calcium oxide nanoparticles (T = 1000 °C, t = 6 hours)

Dewi et al. (2023) identified that calcium oxide nanoparticles derived from sea shell powder samples exhibit diffraction peaks at angles of 2θ = 32.2°, 37.4°, 53.9°, and 64.3°.

Table 1 presents the phases identified at each 2Θ angle, along with their corresponding intensity, d [A] value, and full width at half maximum (FWHM) value. The diffraction peaks associated with calcium oxide nanoparticles (designated as phase B) were observed with high intensity at angles 2Θ = 47.19° and 29.44°, while lower intensity peaks were detected at angles 2Θ = 39.41°, 43.18°, and 48.55°. Additionally, the presence of calcium hydroxide ($Ca(OH)_2$) (designated as phase A) was confirmed, as indicated by diffraction peaks at angles 2Θ = 18.04°, 28.74°, 34.16°, 50.88°, 54.43°, 59.47°, 62.67°, and 64.39°. The formation of calcium hydroxide compounds occurs due to the strong basic properties of CaO; when exposed to atmospheric conditions, the

Table 1. Diffraction peak values (I/I0) of the intensity of the 2Θ region of calcium oxide nanoparticles

Diffraction peak value				
2theta [Θ]	d [A]	I/I0	FWHM	Phase
18.04	4.9124	508.09	0.4826	A
28.74	3.1039	230.97	0.3353	A
29.44	3.0315	109.20	0.3802	B
34.16	2.6227	1000.00	0.4303	A
36.95	2.4308	8.33	0.4400	
39.41	2.2845	24.38	0.4197	B
43.18	2.0933	24.04	0.3066	B
47.19	1.9243	336.36	0.5280	A, B
48.55	1.8738	33.36	0.6714	B
50.88	1.7934	364.56	0.3632	A
54.43	1.6845	164.35	0.4347	A
59.47	1.5531	29.96	0.3783	A
62.67	1.4813	108.18	0.4693	A
64.39	1.4458	79.33	0.6716	A

water vapor (H_2O) in the air reacts with CaO to yield $Ca(OH)_2$ (Harsha Hebbar et al., 2018). Furthermore, Vijai Anand et al. (2021) suggest that the presence of calcium hydroxide compounds during the synthesis of calcium oxide nanoparticles is attributable to humid environmental conditions, which facilitate the contamination of calcium oxide with water vapor.

The miller index values (h, k, l) and lattice planes of the diffraction peaks of calcium oxide nanoparticles (phase B) is illustrated in Table 2.

Based on the data presented in Table 2, the crystal peak distribution of calcium oxide nanoparticles (Phase B) exhibits distinct lattice plane indices, specifically at angles 2Θ = 29.44° (plane 200), 39.41° (plane 220), 43.18° (plane 311), 47.19° (plane 220), and 48.55° (plane 400). Reference to the JCPDS/ICDD standard diffraction pattern database (Joint Committee on Powder Diffraction Standards/International Center for Diffraction Data) indicates that the primary diffraction peaks for calcium oxide occur at angles 2Θ in the range of 32.2° to 37° (corresponding to the 111–200 planes), 53.9° (220 plane), and 64.2° to 67.5° (222–311 planes). The resultant crystal structure demonstrates uniformity across all diffraction peak distributions of calcium oxide nanoparticles, which exhibit a face-centered cubic (FCC) structure (El-Sherif et al., 2023). Li et al. (2022) explain that the synthesis of calcium oxide nanoparticles from limestone using a thermal method yields nanoparticles with a face-centered cubic crystal morphology. The FCC crystal structure of the calcium oxide nanoparticles is illustrated in Figure 5.

Figure 5 illustrates the face-centered cubic crystal structure of calcium oxide nanoparticles and the associated atomic components. The crystal structure of calcium oxide nanoparticles is characterized by a FCC configuration, which includes one atom positioned at each corner of the cube, along with additional atoms located at the midpoints of each face of the cube (Raza et al., 2024). This observation is consistent with the findings of Lai et al. (2020), who identified the crystal structure of calcium oxide as FCC through X-ray diffraction analysis.

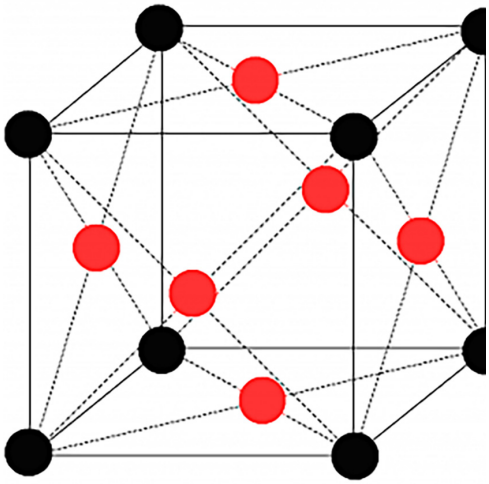

Figure 5. FCC crystal shape of calcium oxide nanoparticles

Particle size values derived from X-ray diffraction data can be ascertained utilizing the Scherrer equation. This equation facilitates the determination of crystal particle size based on the width of the resulting diffraction peak (Maringgal et al., 2020). The parameters employed in calculating particle size using the Scherrer equation include the Scherrer constant (K = 0.9–1), X-ray wavelength (λ), full width at half maximum (FWHM) value (β), and the Bragg angle, which represents half of the diffraction angle (2Θ) (Θ). The particle size values for calcium oxide nanoparticles are presented in Table 3.

Based on Table 3, calcium oxide nanoparticles exhibit an average particle size of 24.87 nm. This measurement is derived from the diffraction angle within the 2θ region of the calcium oxide

Table 2. Miller index values (*h*, *k*, *l*) and lattice planes of the diffraction peaks of calcium oxide nanoparticles (phase B)

CaO compound parameters (Phase B)					
2Θ (°)	Θ (°)	d[Å]	Index miller (h,k,l)	Grid field value	Crystal shape
47.19	23.59	1.923	6	220	Face centered cubic (FCC)
29.44	14.72	3.034	2	200	Face centered cubic (FCC)
39.41	19.705	2.284	4	220	Face centered cubic (FCC)
43.18	21.59	2.093	6	311	Face centered cubic (FCC)
48.55	24.275	1.876	8	400	Face centered cubic (FCC)

Table 3. Particle size values of calcium oxide nanoparticles using the Scherrer equation

2Θ (°)	Θ (°)	FWHM	Particle size/D (nm)	Average particle size (nm)
29.44	14.72	0.3802	21.60	24.87
39.41	19.70	0.4197	20.11	
43.18	21.59	0.3066	27.87	
47.19	23.59	0.5280	25.48	
48.55	24.27	0.6714	29.30	

nanoparticles, specifically utilizing the θ value and the full width at half maximum (FWHM) value in conjunction with the Scherrer equation (Alobaidi et al., 2022). According to SNI ISO/TS 80004-4:2013, materials possessing nanosized structures are characterized by an internal shape or surface structure with crystal sizes ranging from 1 to 100 nm. This classification confirms that calcium oxide nanoparticles fall within the nanoscale category as defined by established standards. Alobaidi et al. (2022) synthesized calcium oxide nanoparticles from eggshell waste, achieving a particle size ranging from 20 to 70 nm, as determined through scanning electron microscopy and X-ray diffraction analysis. Additionally, Mazher et al. (2023) synthesized calcium oxide nanoparticles via a green chemical method utilizing Citrullus colocynthis fruit extract, resulting in a particle size measurement of 53.93 ± 2.54 nm, as calculated using XRD techniques.

Characterization of CaO nanoparticles using SEM

Scanning electron microscopy characterization was conducted to ascertain the particle surface morphology of calcium oxide nanoparticles (CaO-NPs) (M et al., 2023). Jadhav et al. (2022) suggest that SEM can be utilized to determine the morphology and surface characteristics of a material by employing a high-frequency electron beam, thereby enabling the instrument to capture these features in a visual format. The SEM instrument employed in this study was the Hitachi SU3500, operating at a voltage of 15 kV. The morphology of the calcium oxide nanoparticles is illustrated in Figure 6.

Based on Figure 6, CaO nanoparticles exhibit a non-uniform surface morphology and are predominantly spherical in shape. This characteristic is attributable to the diminutive size of CaO nanoparticles, which results in a high surface area-to-volume ratio. Consequently, the Van der Waals forces between the particles become significantly pronounced, promoting the tendency for these particles to adhere to one another and form agglomerates. Furthermore, the synthesis of CaO nanoparticles utilizing a green chemistry approach that employs water (H_2O) as a solvent leads to an increased propensity for calcium oxide to absorb water vapor. This absorption facilitates the formation of a thin layer on the surface of the nanoparticles, acting as a capillary bridge that further contributes to agglomeration (Ren et al., 2023). Additionally, Ali et al. (2023) noted that calcium oxide nanoparticles demonstrate an agglomerated surface morphology with a spherical shape, as determined through scanning electron microscopy analysis.

Isolation of gram-positive and negative bacteria in wastewater

Wastewater samples were collected from five designated sampling points within the domestic landfill area located in Antang, Manggala Village, Makassar, Indonesia (Bintang et al., 2023). Each sample was assigned a code corresponding to its

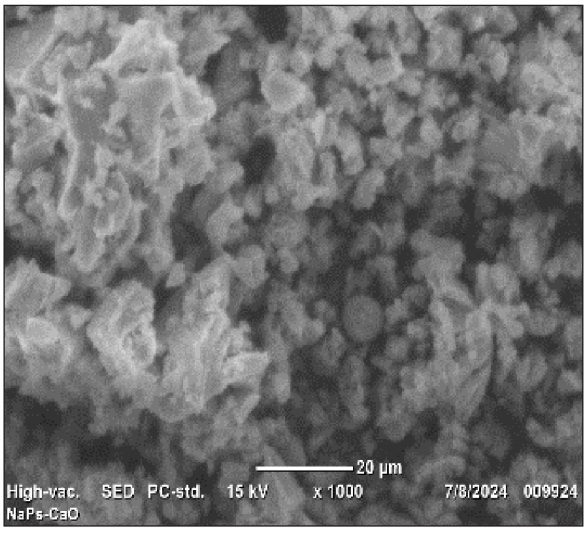

Figure 6. Morphology of calcium oxide nanoparticles at 1000x magnification

respective collection station, designated as S1, S2, S3, S4, and S5. The samples were prepared and analyzed in the laboratory to ensure their integrity prior to further experimentation. The subsequent phase involved dilution at a ratio of 10^{-1}, aimed at mitigating the proliferation of microbial colonies, thereby facilitating their isolation (Chandra, 2023). According to Zhou et al. (2024), bacterial isolation is conducted through various stages to yield isolates that are amenable to cultivation and produce colonies that are not excessively large on the culture medium as a result of the dilution process. Consequently, dilution is essential for fostering colonies that can proliferate effectively. The isolated wastewater samples from the five stations are depicted in Figure 7.

Identification of *Escherichia coli* bacteria

The isolation and identification test of Gram-negative bacteria, specifically *Escherichia coli*, aims to elucidate the interpretative results derived from the examination of EMBA media scratches. Positive results are indicated by the emergence of a metallic greenish-black coloration at the center of the colonies observed on EMBA media (Costinar et al., 2022). According to Wang et al. (2024), EMBA media encompasses lactose, which facilitates differentiation among bacterial groups based on their lactose fermentation capabilities. *Escherichia coli* is a notable bacterium that can ferment lactose. This species is characterized by its rapid and efficient lactose fermentation, resulting in sufficient acid production to yield a distinctive metallic green coloration of the colonies (Xiao et al., 2024). The outcomes of the isolation and identification tests for *Escherichia coli* on EMBA media, derived from wastewater samples, are presented in Table 4.

Based on Table 4, the colonies that proliferated on MBA media were identified as gram-negative *Escherichia coli*, characterized by the presence of metallic green colonies. Sample codes S1, S2, S3, S4, and S5 all exhibited positive results for the presence of *Escherichia coli*, as evidenced by the identification of metallic green coloration in each sample (Zhou et al., 2024). Furthermore, Xiao et al. (2024) suggest that the isolation of *Escherichia coli* from well water, following growth on EMBA media, results in the formation of metallic green colonies subsequent to the incubation process. The overgrowth of metallic green colonies on MBA media is illustrated in Figure 8.

Biochemical test results of gram-negative bacteria *Escherichia coli*

Indole production test

Indole production tests utilizing tryptone broth media serve to assess the capacity of *Escherichia coli* to metabolize the amino acid tryptophan into indole. The presence of indole can be detected through the application of Kovac's reagent (Takci et al., 2024). The introduction of Kovac's reagent is intended to identify the formation of a red ring at the surface of the media following its reaction with indole (Shultana and Khan, 2022). According to Han et al. (2019), Kovac's reagent comprises

Figure 7. Wastewater samples based on 5 station points

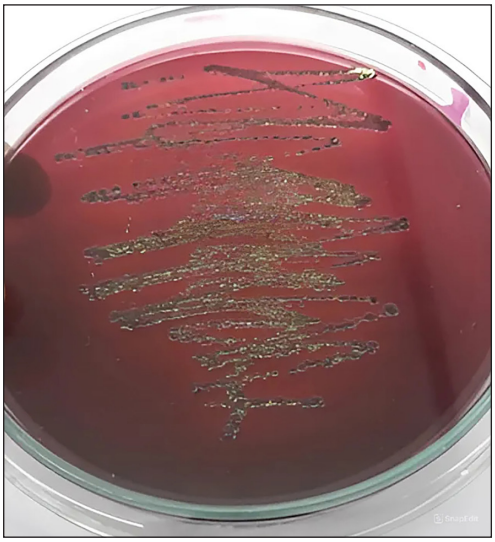

Figure 8. MBA media with metallic green colonies

Table 4. Isolation results on EMBA media of wastewater samples

Sample code	Color of colonies growing on EMBA media	Description
S1	Metallic green colonies	+
S2	Metallic green colonies	+
S3	Metallic green colonies	+
S4	Metallic green colonies	+
S5	Metallic green colonies	+

Note: (+) = positive for *Escherichia coli* bacteria.

dimethylaminobenzaldehyde compounds that react with indole to yield a bright red or pink complex, thereby facilitating analysis within the media. The results of the indole test conducted on wastewater samples are presented in Table 5.

Based on Table 5, the indole results from sample codes S1 to S5, tested with covac reagent, yielded positive outcomes indicated by the formation of a red ring-shaped layer at the surface of the medium (Wichmann et al., 2021). Kim et al. (2020) reported that bacterial isolates of gram-negative Enterobacteriaceae in industrial wastewater samples exhibited negative results in the indole test; specifically, 10 isolates produced black sediment, while 5 isolates did not yield any black coloration. The presence of a black precipitate signifies that the microorganisms are capable of producing H2S compounds. Indole has the ability to interact with aldehydes and is indicative of Escherichia coli, which possesses the capability to degrade amino acids (Takci et al., 2024). According to Chandra et al. (2023), the indole reaction with *Escherichia coli* can be employed to assess the organism's ability to metabolize the amino acid tryptophan into indole via the enzyme tryptophanase. This conversion can be further validated using covac reagent, resulting in a pink or red coloration at the surface of the medium. The results of the indole production test are depicted in Figure 9.

Methyl Red test

The Methyl Red test is designed to assess the capacity of organisms to maintain stable acidic byproducts resulting from glucose fermentation (Wang et al., 2024). Xiao et al. (2023) suggest that the Methyl Red test can evaluate the ability of bacteria to utilize the glucose fermentation pathway, as indicated by the presence of an acidic mixture with a low pH (< 4.4). The results of the Methyl Red test conducted on wastewater samples are presented in Table 6.

Based on Table 6, the results of the methyl red test indicate that sample codes S1 to S5 exhibit positive test outcomes, as evidenced by a color change from yellow to red on the surface

Figure 9. Observation result of indole production test

Table 5. Indole test results of wastewater samples

Sample code	Comparison of media surface color		Description
	Before Covac reagent is applied	After the Covac reagent is applied	
S1	Black	Red-colored ring shape	+
S2	Black	Red-colored ring shape	+
S3	Black	Red-colored ring shape	+
S4	Black	Red-colored ring shape	+
S5	Black	Red-colored ring shape	+

Note: (+) = positive for *Escherichia coli* bacteria**.**

of the medium following exposure to methyl red (MR) reagent. This finding suggests that sample codes S1, S2, S3, S4, and S5 contain the gram-negative bacteria *Escherichia coli*. According to Wang et al. (2024), *E. coli* can be identified using media that undergoes a color change to red upon contact with methyl red, which occurs through a series of biochemical reactions. Methyl red functions as a pH indicator, exhibiting a red color at a pH of 4.4 or below (Xiao et al., 2024). The results of the methyl red (MR) test are illustrated in Figure 10.

Citrate test

The citrate test is conducted using Koser Citrate Broth (KCB) media. This medium is utilized to determine an organism's ability to utilize citrate as the sole carbon source for energy (Shultana and Khan, 2022). Wang et al. (2024) elucidate that KCB media contains only citrate as the exclusive carbon source, enabling bacteria to utilize citrate as a substrate for their growth. The results of the citrate test conducted on wastewater samples are presented in Table 7.

Based on the data presented in Table 7, the citrate test results indicate that sample codes S1, S2, S3, S4, and S5 exhibit negative outcomes both prior to and following incubation. The negative observation for the citrate test suggests that Escherichia coli bacteria do not utilize citrate as a carbon source, resulting in no color change in the citrate test medium (Raj et al., 2020). Costinar et al. (2022) propose that the use of Simmon's Citrate agar is a method for assessing the carbon utilization capabilities of microorganisms, with results that may be interpreted as positive or negative based on the transition of the medium from green to blue. The observational results of the citrate test conducted on wastewater samples are illustrated in Figure 11.

Indentification of *Staphylococcus aureus* bacteria in wastewater

The isolation and identification of the gram-positive bacterium Staphylococcus aureus will be conducted utilizing Blood Agar Plate (BAP) media (Almwafy, 2020). This medium is designed to incorporate lithium chloride, which is present in wastewater samples, to inhibit the growth of Staphylococcus bacterial colonies and to eliminate any viable bacteria (Chandra, 2023). According to Garcia et al. (2021), BAP media is composed of 5–10% animal blood, which supplies essential nutrients necessary for the growth of certain microorganisms. Furthermore, this medium serves as a

Figure 10. Methyl red (MR) test observation results

Figure 11. Citrate test observations on wastewater samples

Table 6. Methyl Red test results on wastewater samples

Sample code	Comparison of media colors		Description
	Before the reagent is applied	After the reagent is applied	
S1	Yellow	Red circles on the media surface	+
S2	Yellow	Red circles on the media surface	+
S3	Yellow	Red circles on the media surface	+
S4	Yellow	Red circles on the media surface	+
S5	Yellow	Red circles on the media surface	+

Note: (+) = positive for *Escherichia coli* bacteria.

Table 7. Citrate test results on wastewater samples

Sample code	Media discoloration		Description
	Before	After	
S1	Green	Green	-
S2	Green	Green	-
S3	Green	Green	-
S4	Green	Green	-
S5	Green	Green	-

valuable tool for observing hemolytic activity, a characteristic that is crucial for the identification and differentiation of bacterial species. The results obtained from testing *Staphylococcus aureus* on BAP media are presented in Table 8.

Based on Table 8, the results of the *Staphylococcus aureus* bacterial testing on wastewater samples indicate the presence of *Staphylococcus aureus*. Samples S1, S2, S3, S4, and S5 each exhibited black colonies with a round morphology upon examination on blood agar plate (BAP) media (Li et al., 2020). According to Chandra et al. (2023), the characteristics of *Staphylococcus aureus* colonies include a bacterial morphology resembling fingers, with a diameter ranging from 2 to 3 mm and a typical gray coloration. These colonies are surrounded by a clear zone, which creates a distinct bright area on the media. The observation results confirming the presence of *Staphylococcus aureus* on BAP media are illustrated in Figure 12.

Biochemical test results of gram-positive bacteria Staphylococcus aureus

Gram stain test

Bacterial colonies derived from Blood Agar Plate (BAP) media are subjected to gram staining and morphological identification to isolate the desired gram-positive bacteria. Staphylococcus aureus is a type of gram-positive bacterium characterized by its clustered coccus morphology. These distinguishing features are readily

Table 8. *Staphylococcus aureus* bacteria test results on BAP media

Sample code	Observation results on BAP media	Description
S1	Black colonies, round shape	+
S2	Black colonies, round shape	+
S3	Black colonies, round shape	+
S4	Black colonies, round shape	+
S5	Black colonies, round shape	+

Note: (+) = *Staphylococcus aureus* positive category.

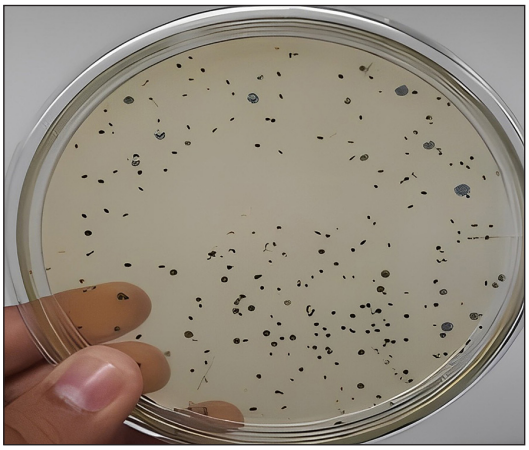

Figure 12. Positive test of Staphylococcus Aureus on BAP media

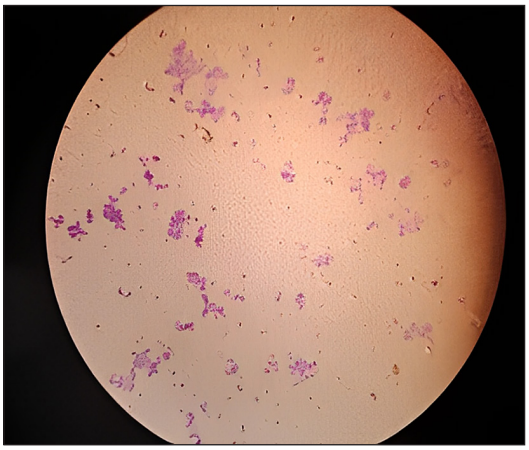

Figure 13. Gram stain identification test of Staphylococcus Aureus bacteria using a microscope

observable when the bacterial isolate undergoes gram staining (Li et al., 2020). The results of the gram staining identification test for *Staphylococcus aureus*, examined under a 100x magnification microscope, are presented in Figure 13.

Based on Figure 13, the results of gram staining conducted on bacterial isolates from wastewater samples, observed under a 100x magnification microscope, indicated that the samples on the glass slide contained bacterial colonies belonging to the gram-positive group. Furthermore, the observed bacteria exhibited a purple, coccus-shaped morphology and a clustered arrangement, allowing for their classification as *Staphylococcus aureus* (Almwafy, 2020). Li et al. (2020) describe gram-positive bacteria, such as *Staphylococcus aureus*, as possessing a coccus shape, while Lowry (1998) characterizes their bacterial cell structure as purple and clustered.

Coagulase test

The coagulase test serves to identify bacteria that produce extracellular type proteins characteristic of Staphylococcus aureus, which are capable of coagulating plasma (Raj et al., 2020). The results of the coagulase test are illustrated in Figure 14.

Based on Figure 14, the results of the coagulase test on samples S1, S2, S3, S4, and S5 indicate positive results for the presence of *Staphylococcus aureus*, which is characterized by the formation of coagulant or bubble clumping at the top of the tube. Chandra et al. (2023) conducted observational tests on household wastewater samples and found that the results indicated the presence of Staphylococcus aureus, as evidenced by the formation of gas bubbles in the test tube. The coagulase test results and colony counts of *Staphylococcus aureus* can be observed in Table 9.

Based on the data presented in Table 9, the coagulase test results for samples S1, S2, S3, S4, and S5 indicated the presence of coagulase-positive gram-positive bacteria, specifically Staphylococcus aureus. Furthermore, the colony counts for *Staphylococcus aureus* in samples S1, S2, S3, S4, and S5 were recorded as 234, 176, 338, 254, and 356 CFU/100 mL, respectively. According to the international standards set by the United States Environmental Protection Agency (EPA), the maximum allowable concentration of Staphylococcus aureus in water and recreational water bodies is 100 CFU/100 mL. The European Union (EU) Bathing Water Directive also recommends that the threshold for Staphylococcus aureus in drinking water and pool water remains below 100 CFU (<100) per 100 mL. Additionally, in accordance with the national standard established by PERMENKES No. 32 of 2017, the quality indicator for drinking water and the threshold for

Table 9. Coagulase test results and colony counts of *Staphylococcus aureus* bacteria

Sample code	Coagulase result of *Staphylococcus aureus* bacteria	Number of colonies of *Staphylococcus aureus* bacteria (CFU/100 mL)
S1	+	234
S2	+	176
S3	+	338
S4	+	254
S5	+	356

Note: (+) = *Staphylococcus aureus* positive category.

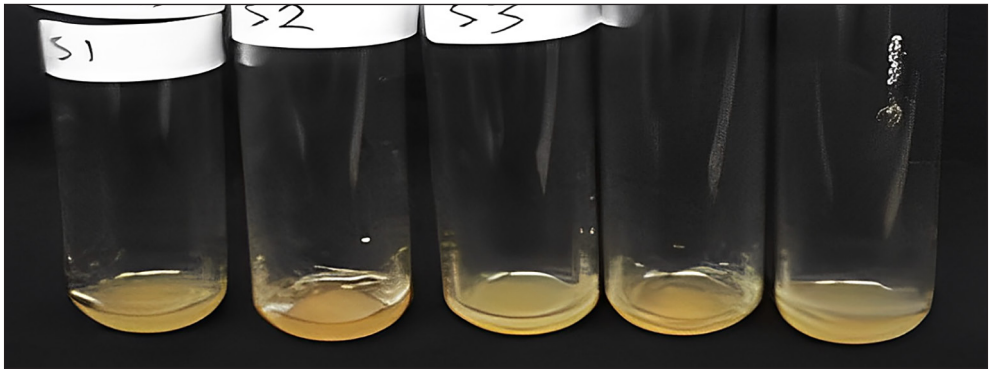

Figure 14. Coagulase test results

contamination by *Staphylococcus aureus* are defined as <100 CFU/100 mL. Based on these established standards, it can be concluded that the wastewater samples collected from the Antang area landfill in Manggala Village, Makassar, Indonesia, exceed both international and national thresholds, measuring >100 CFU/100 mL. Bintang et al. (2023) indicate that *Staphylococcus aureu*s contamination is largely attributable to domestic and industrial waste discharges that accumulate in aquatic environments, potentially leading to significant public health concerns. Furthermore, Aysun et al. (2024) highlight that water contaminated with *Staphylococcus aureus* can result in severe health issues in humans, including abdominal pain, diarrhea, and pruritus. Prolonged exposure to such contamination may lead to serious conditions such as intestinal diseases, urinary tract infections, sepsis, and meningitis. The graphical representation of the *Staphylococcus aureus* colony count results from the wastewater samples is depicted in Figure 15.

Antibacterial activity of CaO nanoparticles

Antibacterial testing was conducted qualitatively, following the methodology established by Wahyuningsih & Lovy (2020) utilizing the disc paper method. The test bacteria employed in this study were Escherichia coli and Staphylococcus aureus, with sterile aqua serving as the positive control and chloramphenicol (30 µL) as the negative control. The experimental procedure involved triplicate replications to assess the diameter of inhibition at 24, 48, and 72 hours. The data pertaining to the antibacterial efficacy of CaO nanoparticles (CaO-NPs) against *Escherichia coli* and *Staphylococcus aureus* are presented in Tables 10 and 11.

Based on Tables 10 and 11, the inhibition zones observed in *Escherichia coli* and *Staphylococcus aureus* bacteria following exposure to calcium oxide nanoparticles exhibited varying results for each concentration. Specifically, an increase in the concentration of calcium oxide nanoparticles corresponded with a larger diameter of the inhibition zone. The average inhibition zones for 1%, 3%, and 5% concentrations of CaO nanoparticles against E. coli were recorded as 9.59, 10.17, and 11.78 mm, respectively, with the positive control (chloramphenicol) measuring 12.65 mm. For *S. aureus*, the average inhibition zones at the same concentrations of CaO

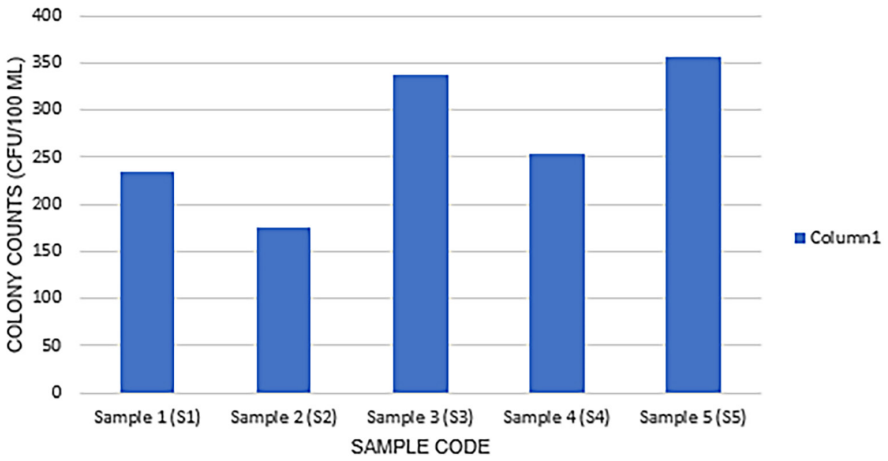

Figure 15. Colony count results of *Staphylococcus aureus* bacteria in wastewater samples

Table 10. The results of determining the inhibition of CaO nanoparticles with *Escherichia coli* test bacteria

Concentration	Inhibition zone diameter (mm)			Average (mm)
	Rep I	Rep II	Rep III	
CaO-NPs 1%	10.55	8.56	9.67	9.59
CaO-NPs 3%	11.28	10.21	10.85	10.78
CaO-NPs 5%	12.60	11.84	10.90	11.78
Control (+) chloramphenicol	14.61	10.56	12.78	12.65
Control (-) sterile aqua	0	0	0	0

Table 11. The results of determining the inhibition of CaO nanoparticles with *Staphylococcus aureus* test bacteria

Concentration	Inhibition Zone Diameter (mm)			Average (mm)
	Rep I	Rep II	Rep III	
CaO-NPs 1%	11.20	9.27	10.31	10.26
CaO-NPs 3%	11.71	11.33	10.42	11.15
CaO-NPs 5%	14.75	13.42	14.29	14.15
Control (+) Chloramphenicol	13.73	11.65	13.10	12.82
Control (-) Sterile Aqua	0	0	0	0

nanoparticles were 10.26, 11.15, and 14.15 mm, with the positive control (chloramphenicol) measuring 12.82 mm. The negative control utilized was sterile water, which was free from microorganism contamination, resulting in a diameter of 0 mm for each replication and each test bacterium (Meng et al., 2024).

The zone of inhibition of CaO nanoparticles at concentrations of 1%, 3%, and 5% against *Escherichia coli* at replication I (24 hours) was measured at 10.55 mm, 11.28 mm, and 12.60 mm, respectively. The growth response of *Escherichia coli* in replication I is classified within the medium-strong category. During this phase, Escherichia coli undergoes an adjustment phase before entering exponential growth, thereby allowing the antibacterial response to function optimally. This is attributed to the rapid division of *Escherichia coli*, during which CaO nanoparticles, as antibacterial agents, interfere with cell wall synthesis, protein synthesis, and DNA replication, effectively inhibiting and killing the bacteria (Djayasinga et al., 2024). In replication II (48 hours), the inhibition zone of CaO nanoparticles at concentrations of 1%, 3%, and 5% exhibited a decrease in diameter, recorded at 8.56 mm, 10.21 mm, and 11.84 mm, respectively. This reduction is due to the *Escherichia coli* entering a stationary phase characterized by a slowdown in bacterial growth, leading to a diminished antibacterial response from the CaO nanoparticles. During this phase, the effectiveness of the antibacterial CaO nanoparticles can decline, as the bacteria are in a slow metabolic state with reduced cell division. Consequently, antibacterial agents targeting active growth processes, such as inhibitors of cell wall and protein synthesis, become less effective. In replication III (72 hours), the inhibition zone of CaO nanoparticles at concentrations of 1%, 3%, and 5% again showed an increase in diameter, measuring 9.27 mm, 10.85 mm, and 10.90 mm, respectively. At this stage, *Escherichia coli* has entered the death phase, resulting in an increased antibacterial response (Jadhav et al., 2022). During the bacterial death phase, antibacterials can directly damage cell membranes and induce cell death, particularly as the metabolic activity of the bacteria is significantly reduced (Abbas and Aadim, 2022). The histogram depicting the inhibition zone of CaO nanoparticles against *Escherichia coli* can be referenced in Figure 16.

In the assessment of *Staphylococcus aureus*, the inhibition zones produced by CaO nanoparticles at various concentrations exhibited a comparable inhibition pattern to that observed with *Escherichia coli*. In Replication I (24 hours), the inhibition zones for CaO nanoparticles at concentrations of 1%, 3%, and 5% were measured at

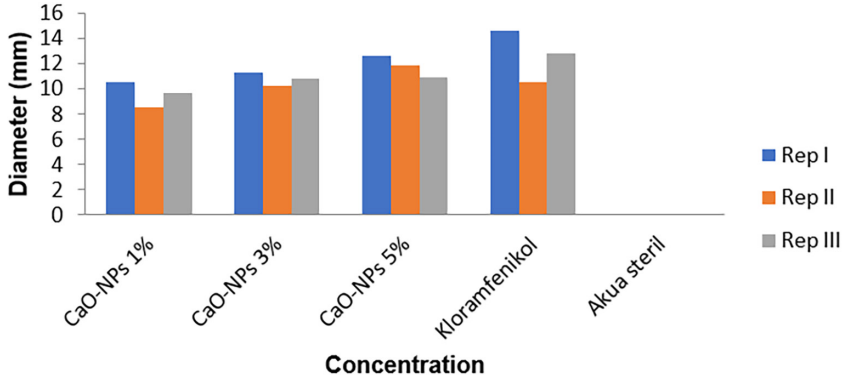

Figure 16. Histogram graph of CaO-NPs inhibition zone against *Escheria coli*

11.20 mm, 11.71 mm, and 14.75 mm, respectively. The antibacterial inhibition observed under these conditions was classified as strong. In Replication II (48 hours), the diameters of the inhibition zones for the same concentrations of CaO nanoparticles decreased compared to Replication I, recording values of 9.27 mm, 11.31 mm, and 13.42 mm, respectively. The antibacterial inhibition in Replication II was categorized as moderate-strong. In Replication III (72 hours), the inhibition zones for CaO nanoparticles at concentrations of 1%, 3%, and 5% were measured at 10.31 mm, 10.42 mm, and 14.29 mm, respectively. The antibacterial inhibition in Replication III was similarly categorized as moderate-strong. A histogram illustrating the inhibition zones of CaO nanoparticles against Staphylococcus aureus can be found in Figure 17.

The antibacterial activity exhibited by CaO nanoparticles is more effective in inhibiting the growth and eliminating the test bacterium *Staphylococcus aureus* compared to *Escherichia coli* (Ramola and Joshi, 2019). This disparity can be

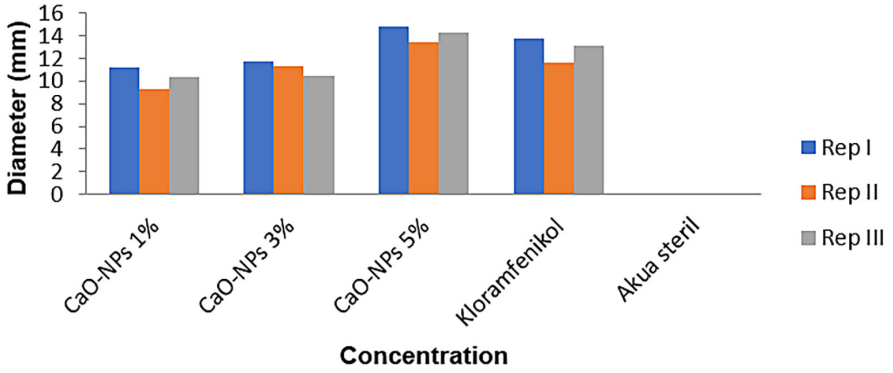

Figure 17. Histogram graph of CaO-NPs inhibition zone against *S. aureus*

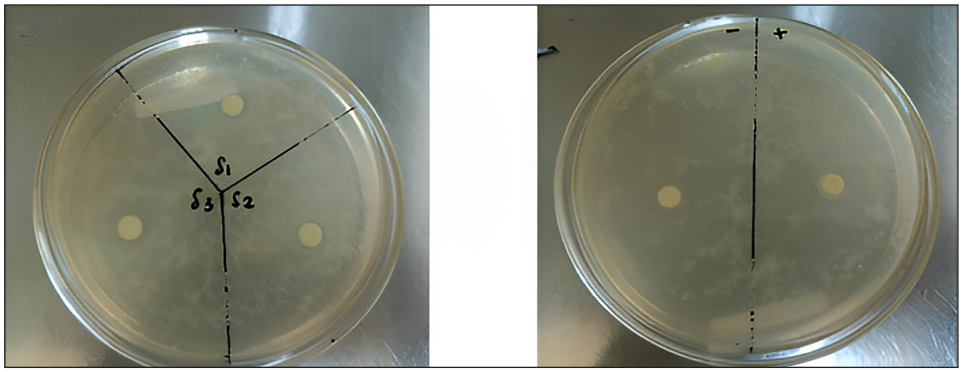

Figure 18. Zone of Inhibition of *S. aureus* bacteria: a) CaO-NPs (1%; 3%, 5%), b) 100 µL chloramphenicol (+), sterile aqua (-)

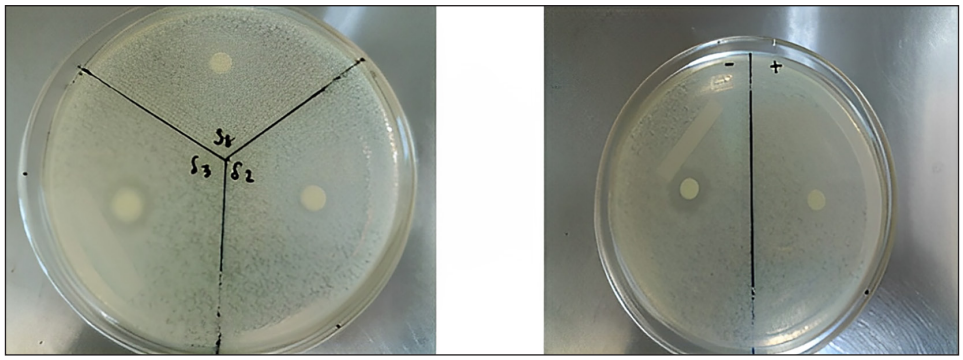

Figure 19. Zone of Inhibition of *E. coli* bacteria: a) CaO-NPs (1%, 3%, 5%), b) 100 µL chloramphenicol (+), sterile aqua (-)

attributed to the classification of *S. aureus* as a gram-positive bacterium, characterized by a simpler cell wall structure that lacks an outer membrane, in contrast to *E. coli*, which possesses a more complex cell wall and an outer membrane containing lipopolysaccharide (LPS). Consequently, the simpler structure of *S. aureus* allows for easier penetration by CaO nanoparticles (Zheng et al., 2019). Furthermore, the absence of an outer membrane in *S. aureus* facilitates the diffusion of CaO nanoparticles into the cell, enabling them to directly damage the cell membrane and other intracellular components (Mbenga et al., 2023). Additionally, CaO nanoparticles can generate reactive oxygen species (ROS), which induce oxidative damage to the cell wall, DNA, and proteins of *S. aureus*, resulting in accelerated cell death (López-Badillo et al., 2021). Furthermore, Alsohaimi et al. (2020) indicated that the antibacterial efficacy of CaO nanoparticles derived from eggshells demonstrates a higher inhibitory effect on *S. aureus* compared to *E. coli*, with inhibition zones measuring 33 mm and 23.33 mm, respectively, at a concentration of 25%. The results of antibacterial tests conducted using the disc diffusion method on gram-positive bacteria (*Staphylococcus aureus*) andgram-negative bacteria (*Escherichia coli*) are illustrated in Figures 18 and 19, respectively.

CONCLUSIONS

Calcium oxide nanoparticles were successfully synthesized with an average particle size of 24.87 nm utilizing green chemistry principles derived from bitti plant extract. The principles of green chemistry enhance the efficiency of nanoparticle synthesis due to their environmentally friendly nature, low operational costs, and rapid synthesis times. Calcium oxide nanoparticles have potential applications as antibacterial agents, particularly in the reduction of microbial waste in water, thereby offering a renewable innovation in water management technology. This development paves the way for researchers to pursue novel breakthroughs in the management of wastewater contaminated by industrial and domestic activities.

Acknowledgements

The author wishes to express gratitude to the primary academic supervisors, Dr. Abdul Karim and Mrs. Nur Umriani Permatasari, for their unwavering support and assistance throughout the research preparation process, as well as for their guidance in the compilation of this article. Additionally, the author acknowledges the contributions of all parties involved in the preparation of this paper, which facilitated its successful completion.

REFERENCES

1. Abbas, I.K., Aadim, K.A., 2022. Synthesis and Study of Structural Properties of Calcium Oxide Nanoparticles Produced by Laser-Induced Plasma and its Effect on Antibacterial Activity. Sci. Technol. Indones. 7. https://doi.org/10.26554/sti.2022.7.4.427-434
2. Ahmad, W., Kamboj, A., Banerjee, I., Jaiswal, K.K., 2022. Pomegranate peels mediated synthesis of calcium oxide (CaO) nanoparticles, characterization, and antimicrobial applications. Inorg. Nano-Metal Chem. https://doi.org/10.1080/24701556.2021.2025080
3. Almwafy, A., 2020. Preliminary characterization and identification of gram positive hemolysis bacteria. Al-Azhar J. Pharm. Sci. 62. https://doi.org/10.21608/ajps.2020.118378
4. Alobaidi, Y.M., Ali, M.M., Mohammed, A.M., 2022. Synthesis of Calcium Oxide Nanoparticles from Waste Eggshell by Thermal Decomposition and their Applications. Jordan J. Biol. Sci. 15. https://doi.org/10.54319/jjbs/150215
5. Aysun Mercimek Takci, H., Sumengen Ozdenefe, M., Buyukkaya Kayis, F., Dincer, S., 2024. Bacteriological Perspective of Water Quality, in: Water Quality - New Perspectives. https://doi.org/10.5772/intechopen.112874
6. Bintang, A., Syafri, M., Rante, A., Marpaung, M.P., Fitrah, F., Putri, S.K., Yusrianto, Y., 2023. Quality of Liquid Waste at the General Hospital in Makassar. Int. J. Health Sci. (Qassim). 1. https://doi.org/10.59585/ijhs.v1i4.181
7. Bôlla de Menezes, L., Cristine Ladwig Muraro, P., Moro Druzian, D., Patricia Moreno Ruiz, Y., Galembeck, A., Pavoski, G., Crocce Romano Espinosa, D., Leonardo da Silva, W., 2024. Calcium oxide nanoparticles: Biosynthesis, characterization and photocatalytic activity for application in yellow tartrazine dye removal. J. Photochem. Photobiol. A Chem. 447. https://doi.org/10.1016/j.jphotochem.2023.115182
8. Chandra, M.A., 2023. Identification of bacterial morphology and catalase coagulation test on propionibacterium acnes bacteria. J. Heal. Manag. Pharm. Explor. 1. https://doi.org/10.52465/johmpe.v1i2.152
9. Costinar, L., Herman, V., Pitoiu, E., Iancu, I., Degi, J., Hulea, A., Pascu, C., 2022. Boar semen contamination: Identification of gram-negative bacteria and antimicrobial resistance profile. Animals 12. https://doi.org/10.3390/ani12010043

10. Dewi, D.K., Putri, V.M., Febriyanti, V., Yudha, C.S., 2023. Calcination of Various Eggshell Wastes into CaO Heterogeneous Catalysts. Equilib. J. Chem. Eng. 7. https://doi.org/10.20961/equilibrium.v7i1.74484
11. Djayasinga, R., Situmeang, R.T.M., Unob, F., Hadi, S., Manurung, P., Sumardi, S., 2024. Chicken Eggshell Powder as Antibacterial Against Staphylococcus aureus and Escherichia coli Through In Vitro Studies. J. Multidiscip. Appl. Nat. Sci. 4. https://doi.org/10.47352/jmans.2774-3047.205
12. Dobrzynska, M., Napierala, M., Florek, E., 2020. Flavonoid nanoparticles: A promising approach for cancer therapy. Biomolecules. https://doi.org/10.3390/biom10091268
13. El-sherif, A.A., Hamad, A.M., Shams-Eldin, E., Mohamed, H.A.A.E., Ahmed, A.M., Mohamed, M.A., Abdelaziz, Y.S., Sayed, F.A.Z., El qassem Mahmoud, E.A.A., Abd El-Daim, T.M., Fahmy, H.M., 2023. Power of recycling waste cooking oil into biodiesel via green CaO-based eggshells/Ag heterogeneous nanocatalyst. Renew. Energy 202. https://doi.org/10.1016/j.renene.2022.12.041
14. Garcia, B.L.N., Fidelis, C.E., Freu, G., Granja, B. de M., dos Santos, M.V., 2021. Evaluation of Chromogenic Culture Media for Rapid Identification of Gram-Positive Bacteria Causing Mastitis. Front. Vet. Sci. 8. https://doi.org/10.3389/fvets.2021.662201
15. Han, J.Y., Wiederoder, M., DeVoe, D.L., 2019. Isolation of intact bacteria from blood by selective cell lysis in a microfluidic porous silica monolith. Microsystems Nanoeng. 5. https://doi.org/10.1038/s41378-019-0063-4
16. Harsha Hebbar, H.R., Math, M.C., Yatish, K. V., 2018. Optimization and kinetic study of CaO nanoparticles catalyzed biodiesel production from Bombax ceiba oil. Energy 143. https://doi.org/10.1016/j.energy.2017.10.118
17. Jadhav, V., Bhagare, A., Wahab, S., Lokhande, D., Vaidya, C., Dhayagude, A., Khalid, M., Aher, J., Mezni, A., Dutta, M., 2022. Green Synthesized Calcium Oxide Nanoparticles (CaO NPs) Using Leaves Aqueous Extract of Moringa oleifera and Evaluation of Their Antibacterial Activities. J. Nanomater. 2022. https://doi.org/10.1155/2022/9047507
18. Jiang, B., Xia, D., Yu, B., Xiong, R., Ao, W., Zhang, P., Cong, L., 2019. An environment-friendly process for limestone calcination with CO2 looping and recovery. J. Clean. Prod. 240. https://doi.org/10.1016/j.jclepro.2019.118147
19. Khan, A.U., Hussain, T., Abdullah, Khan, M.A., Almostafa, M.M., Younis, N.S., Yahya, G., 2023. Antibacterial and Antibiofilm Activity of Ficus carica-Mediated Calcium Oxide (CaONPs) Phyto-Nanoparticles. Molecules 28. https://doi.org/10.3390/molecules28145553
20. Kim, H.R., Song, M.Y., Chan Kim, B., 2020. Rapid isolation of bacteria-specific aptamers with a non-SELEX-based method. Anal. Biochem. 591. https://doi.org/10.1016/j.ab.2019.113542
21. Kumar, S., Sharma, V., Pradhan, J.K., Sharma, S.K., Singh, P., Sharma, J.K., 2021. Structural, optical and antibacterial response of CaO nanoparticles synthesized via direct precipitation technique. Nano Biomed. Eng. 13. https://doi.org/10.5101/NBE.V13I2.P172-178
22. Lai, L., Imai, T., Umezu, M., Ishii, M., Ogura, H., 2020. Possibility of calcium oxide from natural limestone including impurities for chemical heat pump. Energies 13. https://doi.org/10.3390/en13040803
23. Li, D., Wang, Y., Li, Z., 2022. Limestone Calcination Kinetics in Microfluidized Bed Thermogravimetric Analysis (MFB-TGA) for Calcium Looping. Catalysts 12. https://doi.org/10.3390/catal12121661
24. Li, H., Li, L., Chi, Y., Tian, Q., Zhou, T., Han, C., Zhu, Y., Zhou, Y., 2020. Development of a standardized Gram stain procedure for bacteria and inflammatory cells using an automated staining instrument. Microbiologyopen 9. https://doi.org/10.1002/mbo3.1099
25. Li, Y., Lou, D., Zhou, X., Zhuang, X., Wang, C., 2024. Alteration of bacterial community composition in the sediments of an urban artificial river caused by sewage discharge. PeerJ 12. https://doi.org/10.7717/peerj.16931
26. López-Badillo, C.M., Hernández-González, M., Hernández-Centeno, F., Olivas-Armendáriz, I., Rodríguez-González, C.A., Múzquiz-Ramos, E.M., López-Cuevas, J., López-De la Peña, H.Y., 2021. Antibacterial activity and in vitro cytotoxicity studies of Ag-doped CaO nanoparticles. Mater. Lett. 283. https://doi.org/10.1016/j.matlet.2020.128741
27. Lv, S., Li, Y., Zhao, S., Shao, Z., 2024. Biodegradation of Typical Plastics: From Microbial Diversity to Metabolic Mechanisms. Int. J. Mol. Sci. https://doi.org/10.3390/ijms25010593
28. M, K., Sundararaman, S., J, A. kumar, Deivasigamani, P., M, R., 2023. Synthesis and characterization of barium doped CaO heterogeneous nanocatalyst for the production of biodiesel from Catharanthus roseus seeds: Kinetics, optimization and performance evaluation. Environ. Res. 222. https://doi.org/10.1016/j.envres.2023.115336
29. Mahmoud, S.M., Barakat, O.S., Kotram, L.E., 2023. Stimulation the immune response through ξ potential on core–shell 'calcium oxide/magnetite iron oxides' nanoparticles. Anim. Biotechnol. 34. https://doi.org/10.1080/10495398.2022.2111310
30. Maringgal, B., Hashim, N., Tawakkal, I.S.M.A., Hamzah, M.H., Mohamed, M.T.M., 2020. Biosynthesis of CaO nanoparticles using Trigona sp. Honey: Physicochemical characterization, antifungal activity, and cytotoxicity properties. J. Mater. Res. Technol. 9. https://doi.org/10.1016/j.jmrt.2020.08.054

31. Mazher, M., Ishtiaq, M., Hamid, B., Haq, S.M., Mazhar, A., Bashir, F., Mazhar, M., Mahmoud, E.A., Casini, R., Alataway, A., Dewidar, A.Z., Elansary, H.O., 2023. Biosynthesis and characterization of calcium oxide nanoparticles from citrullus colocynthis fruit extracts; their biocompatibility and bioactivities. Materials (Basel). 16, 1–21. https://doi.org/10.3390/ma16072768
32. Mbenga, Y., Mthana, M.S., Mthiyane, D.M.N., Ogunjinmi, O.E., Singh, M., Onwudiwe, D.C., 2023. Facile biosynthesis of CaO nanoparticles using extract of Tulbaghia violacea and evaluation of their antibacterial and cytotoxicity activity. Inorg. Chem. Commun. 151. https://doi.org/10.1016/j.inoche.2023.110581
33. Meng, X., Xu, Z., Wang, C., Patitz, J., Boccaccini, A.R., Burkovski, A., Zheng, K., 2024. Surface engineering of mesoporous bioactive glass nanoparticles with bacteriophages for enhanced antibacterial activity. Colloids Surfaces B Biointerfaces 234. https://doi.org/10.1016/j.colsurfb.2023.113714
34. Nam, S.H., Kim, D., An, S., An, Y.J., 2022. Validation of the paper-disc soil method using soil alga Chlorococcum infusionum to quantitatively determine the toxicity of heavy metals. Comp. Biochem. Physiol. Part - C Toxicol. Pharmacol. 258. https://doi.org/10.1016/j.cbpc.2022.109380
35. Nami, Navabeh, Nami, Nasrin, Bostanabad, A.S., 2022. Biosynthesis and Characterization of Fe3O4/CaO Nanoparticles and Investigation of Its Catalytic Property. J. Nanostructures 12. https://doi.org/10.22052/JNS.2022.01.015
36. Rabiei, M., Palevicius, A., Monshi, A., Nasiri, S., Vilkauskas, A., Janusas, G., 2020. Comparing methods for calculating nano crystal size of natural hydroxyapatite using X-ray diffraction. Nanomaterials 10. https://doi.org/10.3390/nano10091627
37. Raj, V.P., Ilakiya, T., Parameswari, E., Davamani, V., 2020. Assessment of New Ecotechnological Measures to Restore the Eutrophicated Lake. Int. J. Curr. Microbiol. Appl. Sci. 9. https://doi.org/10.20546/ijcmas.2020.903.170
38. Ramola, B., Joshi, N.C., 2019. Green Synthesis, Characterisations and Antimicrobial Activities of CaO Nanoparticles. Orient. J. Chem. 35. https://doi.org/10.13005/ojc/350333
39. Raza, H.Z., Shah, A.A., Noreen, Z., Usman, S., Zafar, S., Yasin, N.A., Sayed, S.R.M., Al-Mana, F.A., Elansary, H.O., Ahmad, A., Farzana habib, Aslam, M., 2024. Calcium oxide nanoparticles mitigate lead stress in Abelmoschus esculentus though improving the key antioxidative enzymes, nutritional content and modulation of stress markers. Plant Physiol. Biochem. 206. https://doi.org/10.1016/j.plaphy.2023.108171
40. Ren, H., Zhang, X., Li, Y., Zhang, D., Huang, F., Zhang, Z., 2023. Preparation of Cross-Sectional Membrane Samples for Scanning Electron Microscopy Characterizations Using a New Frozen Section Technique. Membranes (Basel). 13. https://doi.org/10.3390/membranes13070634
41. Sari, Y.C., Junaidi, R., Hasan, A., 2022. Application of limestone as heterogene catalyst for biodiesel production from waste cooking oil. J. Pendidik. dan Teknol. Indones. 2. https://doi.org/10.52436/1.jpti.204
42. Sd, M.K.V., N, C.B., T, V.V.K., N, V., 2023. Beneficiation of low-grade limestone by flotation, in: Materials Today: Proceedings. https://doi.org/10.1016/j.matpr.2022.07.041
43. Shamima Shultana, Ruhul A. Khan, 2022. Water quality assessment, reasons of river water pollution, impact on human health and remediation of polluted river water. GSC Adv. Res. Rev. 10. https://doi.org/10.30574/gscarr.2022.10.2.0053
44. Sharma, H., Lal, R., Pandey, M., Shrivastav, A., 2023. Biosynthesis of CaO nanoparticles using cleome viscosa leaf extract and investigation of their antioxidative and cytotoxicity activity. Orient. J. Chem. 39. https://doi.org/10.13005/ojc/390123
45. Some, S., Mondal, R., Mitra, D., Jain, D., Verma, D., Das, S., 2021. Microbial pollution of water with special reference to coliform bacteria and their nexus with environment. Energy Nexus. https://doi.org/10.1016/j.nexus.2021.100008
46. Wang, X., Patil, N., Li, F., Wang, Z., Zhan, H., Schmidt, D., Thompson, P., Guo, Y., Landersdorfer, C.B., Shen, H.H., Peleg, A.Y., Li, J., Song, J., 2024. PmxPred: A data-driven approach for the identification of active polymyxin analogues against gram-negative bacteria. Comput. Biol. Med. 168. https://doi.org/10.1016/j.compbiomed.2023.107681
47. Wichmann, C., Rösch, P., Popp, J., 2021. Isolation of bacteria from artificial bronchoalveolar lavage fluid using density gradient centrifugation and their accessibility by Raman spectroscopy. Anal. Bioanal. Chem. 413. https://doi.org/10.1007/s00216-021-03488-0
48. Xiao, Y.H., Luo, Z.X., Wu, H.W., Xu, D.R., Zhao, R., 2024. Metagenomic next-generation sequencing for the identification of infections caused by Gram-negative pathogens and the prediction of antimicrobial resistance. Lab Med. 55. https://doi.org/10.1093/labmed/lmad039
49. Zheng, K., Balasubramanian, P., Paterson, T.E., Stein, R., MacNeil, S., Fiorilli, S., Vitale-Brovarone, C., Shepherd, J., Boccaccini, A.R., 2019. Ag modified mesoporous bioactive glass nanoparticles for enhanced antibacterial activity in 3D infected skin model. Mater. Sci. Eng. C 103. https://doi.org/10.1016/j.msec.2019.109764
50. Zhou, Y., Li, J., Li, Z., Yin, H., Zhu, S., Chen, Z., 2024. Rapid and robust bacterial species identification using hyperspectral microscopy and gram staining techniques. J. Biophotonics 17. https://doi.org/10.1002/jbio.202300449